Collision monitoring of manipulators based on variational mode decomposition

She Yingying[1], Wang Gao [2], and Min Feiyan [2,*]

[1]Wuhan Second Ship Design and Research Institute, Wuhan 430205, China

[2]School of Information Science and technology, Jinan University, Guangzhou 510632, China

[*]Correspondence

E-mail: feiyanmin@jnu.edu.cn

Abstract. Collision detection and identification is an important subject for industrial robot research, such as contact location, touching a person or metal, etc. In this paper, a model independent collision detection method is presented, based on the variational mode decomposition of vibration signals generated by collisions. Firstly, the vibration modal features of the manipulator related to collision shock, collision direction and contact position are analysed with dynamic models. Then, the non-stationary vibration symptoms of collisions are extracted with a variational mode decomposition algorithm. The vibration modal symptoms are utilised for the construction and training of the artificial neural network for the collision detection, locating and classification. Finally, the proposed method is validated with both a two-link planar robot. The experimental results show the validity of the collision detection and identification scheme, which can achieve considerable performance.

Keywords: manipulator, collision detection, variational mode decomposition, neural network

1. Introduction

Physical interaction between human and manipulator has become an important topic in robotics research. The aim is to realize safe robot system in unstructured environment and to minimize the risk of injury caused by collisions between human and robot parts[1].

The collision event pipeline is introduced in [2] to divide collision monitoring into multiple phases, including precollision, detection, isolation, identification, classification and response, etc. Collision detection is the second phase of the pipeline, which determines whether a collision has occurred with motor side measurement or torque sensor. Collision isolation is the third stage, and it aims at localizing which part of the robot has collided, so as to let robot react in the most appropriate manner. Besides, based on the information generated in the previous phases, we can interpret the collision nature in a context-dependent way, including the direction of the collision force, accidental or deliberate collision, light or severe, and its time course as permanent or transient [2]. Based on this information, the robot can make reasonable reaction to collision events.

Researchers have addressed the issue of detection the possible collisions of robotic arms . The most commonly used method is the so-called model-based method which compare the actual motor torque with the nominal torque predicted by the robot dynamics model[3][4][5]. Other monitoring methods include sensitive skins [6], safety trajectories [7] and machine learning[8, 9], and so on. A major problem within these model-based methods is the modeling uncertainty on monitoring signal, The uncertainty usually dues to the friction varying with the environment, the load variation, and so on.

Many methods have been proposed to settle the uncertainty and noise of monitoring signals. The momentum observer and velocity observer methods do not need to calculate the acceleration and thus reduce the influence of measurement noise[2]. Literature [3] defines a dynamic threshold that uses fuzzy logic rules to approximate residual dependence on the robot's state (position, velocity, acceleration). In [10][11], the author proposes an adaptive threshold adjustment mechanism for rigid robot and flexible joint robot. In [12, 13], the extended observer method was proposed to improve the rate of convegence.

A worthwhile alternative is to use vibration symptoms to monitor the collision of the manipulator.

The response of robots under collision conditions has a wide spectrum and the response data provides a promising solution for the recognition of collision characteristics. There are many kinds of information about collision events in multi-dimensional high-frequency collision signals, including collision direction, collision location, collision material, collision duration, etc. The time and frequency analysis of collision signals provide a new idea for collision detection and isolation. Another advantage of vibration monitoring is that the method can detect and separate very short time duration collisions, which is an important supplement to the traditional observer method. Besides, the vibration spectrum and modal shape characteristics are relatively fixed and have strong robustness to load and environment changes.

For manufacturing robot, The uncertainty of friction

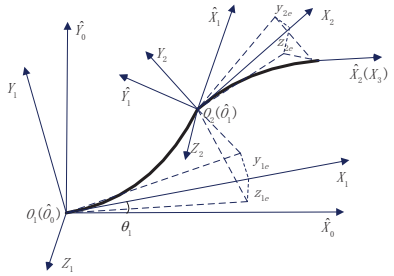


Fig. 1. Coordinate system for planar robot

and gravity is more complex, and the application of the observer method is more difficult. However, collision detection of this kind of robot often relies on the motor side measurements, which represents a practical situation for a large number of industrial robots under the constraints of integration and cost. The method of vibration signal monitoring is especially suitable for this kind of robot.

2. Vibration response and features analysis of robot under collisions

This section presents the primary features which can reveal the inherent relationship between the vibration signals and the collision related information, such as collision occurrences, contact position and materials, using a mathematical way.

2.1. Dynamic equation of robot link

For the sake of simplification, the vibration features of robot is usually studied based on dynamic model two-link planar robot The mathematical model is developed with the following assumptions: (1) Each link is modelled as Euler-Bernoulli beams of uniform density and constant flexural rigidity; (2) the small elastic deformation in both the links as compared to the length of the link. Both of the links is powered by servomotor and move in the vertical plane $\hat{X}_0\hat{O}_0\hat{Y}_0$. Let $(x_i, y_i, z_i(x_i))^T$ be the position of a point along link i with respect to frame (X_i, Y_i, Z_i). The coordinate system of manipulator is presented in Fig. 1.

We considered the vibration characteristic of each link, the deformation $y_i(x_i,t)$ and $z_i(x_i,t)$ satisfying the partial differential equation:

$$\begin{cases} E_i I_{yi}\frac{\partial^4 y_i(x_i,t)}{\partial x_i^4} + E_i I_{yzi}\frac{\partial^4 z_i(x_i,t)}{\partial x_i^4} + \rho_i A_i \frac{\partial^2 y_i(x_i,t)}{\partial t^2} = 0 \\ E_i I_{yzi}\frac{\partial^4 y_i(x_i,t)}{\partial x_i^4} + E_i I_{zi}\frac{\partial^4 z_i(x_i,t)}{\partial x_i^4} + \rho_i A_i \frac{\partial^2 z_i(x_i,t)}{\partial t^2} = 0 \end{cases} \quad (1)$$

where ρ_i is the density of link i, and $E_i I_{yi}, E_i I_{zi}, E_i I_{yzi} (i = 1,2)$ denotes the flexural rigidity respectively.

Considering the separability in time and space of the solution to (1), and the separation of variables method is usually used to solve above equation , i.e.

$$\begin{cases} y_i(x_i,t) = Y_i(x_i)\cdot T_i(t) \\ z_i(x_i,t) = Z_i(x_i)\cdot T_i(t) \end{cases} \quad \cdots\cdots \quad (2)$$

where $T_i(t)$ are the time-variables associated with the assumed spatial mode shape. Referring to the method in literatures [14], the instantaneous deflection is written as

$$\begin{cases} y_i(x_i,t) = \sum_{j=1}^{m_i} Y_{ij}(x_i)\sin(\omega_{ij}t) \\ z_i(x_i,t) = \sum_{j=1}^{m_i} Z_{ij}(x_i)\sin(\omega_{ij}t) \end{cases} \quad \cdots\cdots \quad (3)$$

where $\sin(\omega_{ij}t)$ is the time-varying variables associated with the assumed spatial mode shapes $Y_{ij}(x_i)$ and $Z_{ij}(x_i)$, and j is the number of assumed modes of link i.

Supposing that the collision happens in the y direction of link i, we can get

$$\begin{cases} E_i I_{yi}\frac{\partial^4 y_i(x_i)}{\partial x_i^4} + E_i I_{yzi}\frac{\partial^4 z_i(x_i)}{\partial x_i^4} + \rho_i A_i \frac{\partial^2 y_i(x_i)}{\partial^2 t} = P_y \sin(\omega_j t) \\ E_i I_{yzi}\frac{\partial^4 y_i(x_i)}{\partial x_i^4} + E_i I_{zi}\frac{\partial^4 z_i(x_i)}{\partial x_i^4} + \rho_i A_i \frac{\partial^2 y_i(x_i)}{\partial^2 t} = 0 \end{cases} \quad (4)$$

where ω_j is the exiting frequency of collision, and P_y is the magnitude. The steady state response of this function can be represented as $y_j(x_i) = Y_j(x_i)\sin(\omega_j t)$ and $z_j(x_i) = Z_j(x_i)\sin(\omega_j t)$, and we can get

$$\begin{cases} E[J_z \cdot Y_j^{(4)}(x_i) + J_{yz}\cdot Z_j^{(4)}(x_i)] - \omega_j^2 \rho A_i Y_j(x_i) = P_y \\ E[J_{yz} \cdot Y_j^{(4)}(x_i) + J_z\cdot Z_j^{(4)}(x_i)] - \omega_j^2 \rho A_i Z_j(x_i) = 0 \end{cases} \quad (5)$$

The solution of this equation is found by substituting the trail solution $Y_j(x_i) = C_1 e^{\xi_i x_i}$ and $Z_j(x_i) = C_2 e^{\xi_i x_i}$, the constant coefficient C_1, C_2 is dependent on the boundary conditions of Euler-Bernoulli beams.

$$\begin{cases} E[J_z C_1 Y_j(x_i) + J_{yz} C_2 Z_j(x_i)]\xi_i^4 - \omega_j^2 \rho A_i C_1 Y_j(x_i) = P_y \\ E[J_{yz} C_1 Y_j(x_i) + J_z C_2 Z_j(x_i)]\xi_i^4 - \omega_j^2 \rho A_i C_1 Z_j(x_i) = 0 \end{cases} \quad (6)$$

Since the characteristic roots of this equation is close to $EJ_z\xi_i^4 = \omega_j^2\rho A$ or $EJ_y\xi_i^4 = \omega_j^2\rho A$, and it follows that

$$\begin{aligned} \frac{\ddot{y}_j(x_i)}{\ddot{z}_j(x_i)} &= \frac{(Y_j e^{j\omega_j t})''}{(Z_j e^{j\omega_j t})''} = \frac{Y_j(x_i)}{Z_j(x_i)} \\ &= \frac{C_2 EJ_y\xi^4 - C_2\omega_j^2\rho A_i}{C_1 EJ_{yz}\xi^4} = \frac{C_2[EJ_y - EJ_z]}{C_1 EJ_{yz}} \end{aligned} \quad \cdots \quad (7)$$

where J_y and J_z is the inertial moment, and J_{yz} is the inertial product of the cross-section area within each link. Similarly, when the collision happens in the z direction of link i with magnitude P_z, we can get

$$\frac{\ddot{y}_j(x_i)}{\ddot{z}_j(x_i)} = \frac{C_2 EJ_{yz}\xi^4}{C_1 EJ_z\xi^4 - C_1\omega_j^2\rho A_i} = \frac{C_2 EJ_{yz}}{C_1[EJ_z - EJ_y]} \quad (8)$$

By comparing (7)and (8), it can be seen that the collision direction information is involved in the relative magnitude of vibration amplitude of corresponding direction.

In general, the cross section is usually approximately axisymmetric, the value of J_{yz} approaches zero, and is much smaller than J_y and J_z. For this reason, the vibration response ratio $\ddot{y}_j(x_i)/\ddot{z}_j(x_i)$ under exciting frequency ω_j should be selected as a symptom for the detection of collision direction.

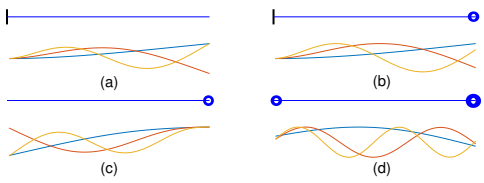


Fig. 2. Vibration modal under different boundary conditions

As the vibration is more sensitive in the collision direction, we further simplify the mathematical model of links in the vibration plane, and its vibration deformation $y_i(x_i,t)$ satisfies the partial differential equation:

$$E_iI_i\frac{\partial^4 y_i(x_i,t)}{\partial x_i^4}+\rho_i\frac{\partial^2 y_i(x_i,t)}{\partial t^2}=0, i=1,2,\cdots,n \quad (9)$$

2.2. Mode shape of single link under collision

Substitute solution (2) to vibration equation (9)

$$\frac{1}{T}\cdot\frac{d^2T_i(t)}{dt^2}=-\frac{1}{Y_i(x_i)}\cdot\frac{d^4Y_i(x_i)}{dx_i^4}\cdot\frac{E_iI_i}{\rho_i}=\omega_i^2 \quad . (10)$$

where ω_i is the natural frequency of link i. We assume that $E_iI_i/\rho_i=a^2$, $\omega_i^2/a^2=\beta_i^4$. Therefore the general solution to () is the product of the time harmonic function

$$T_i(t)=b\sin(\omega_i t+\psi_i) \quad . . . . . (11)$$

and shape function of the form

$$Y_i(x_i)=\begin{array}{l}C_{i1}\cos\beta_i x_i+C_{i2}\sin\beta_i x_i+C_{i3}\\ \cosh\beta_i x_i+C_{i4}\sinh\beta_i x_i\end{array} \quad . . (12)$$

In order to obtain the solution of the mode shape function, proper boundary conditions have to be assumed. These boundary conditions usually include clamped, free or mass connected at the base or at the end of each link .

(1) Link i is clamped at the base, and free at the end. The boundary condition can be described as

$$Y_i(0)=0, Y_i'(0)=0, Y_i''(l_i)=0, Y_i'''(l_i)=0 \quad . . (13)$$

Substitute the above conditions into equation (9),

$$\begin{cases}C_{i1}+C_{i3}=0\\ C_{i2}+C_{i4}=0\\ (\cos\beta_i l_i+\cosh\beta_i l_i)C_{i1}\\ \quad+(\sin\beta_i l_i+\sinh\beta_i l_i)C_{i2}=0\\ (\sin\beta_i l_i-\sinh\beta_i l_i)C_{i1}\\ \quad-(\cos\beta_i l_i+\cosh\beta_i l_i)C_{i2}=0\end{cases} \quad . . . (14)$$

and β_i as a solution to

$$\cos\beta_i l_i\cdot\cosh\beta_i l_i=-1 \quad . . . . . (15)$$

Solving equation(15) for the first three modes gives $\beta_{i1}l_i=1.875$, $\beta_{i2}l_i=4.694$, and $\beta_{i3}l_i=7.855$, and the spatial curve along link i is shown as (a) in Fig. 2.

(2) Link i is clamped at one end, and connected with mass m at the other end. The boundary condition is

$$\begin{array}{ll}Y_i(0)=0 & Y_i'(0)=0\\ Y_i''(l_i)=0 & E_iI_iY_i'''(l_i)=-\omega_i^2mY(l_i)\end{array} \quad . . . (16)$$

We can deduce the transcendental equation about $\beta_i l_i$ as.

$$\frac{M\omega_i^2}{E_iI_i\beta_i^3}=\frac{1+\cos\beta_i l_i\cosh\beta_i l_i}{\sin\beta_i l_i\cosh\beta_i l_i-\cos\beta_i l_i\sinh\beta_i l_i} \quad . (17)$$

where

$$\frac{M\omega_i^2}{E_iI_i\beta_i^3}=\frac{M\beta_i a^2}{(EI)_i}=\frac{M\beta_i l_i}{\rho_i l_i}=\frac{M\beta_i l_i}{m_i} \quad . . . . . (18)$$

The modal shape depends on the mass m_i of link i and connected mass M. As a special case, we assume that $m_i=M$, the spatial curve along link i is as (b).

(3) Link i is free at one end, and connected with mass m at the other end. The boundary condition is

$$\begin{array}{ll}Y_i''(0)=0 & Y_i'''(0)=0\\ Y_i''(l_i)=0 & E_iI_iY_i'''(l_i)=-\omega_i^2mY(l_i)\end{array} \quad . . . (19)$$

The vibration mode equation is:

$$\frac{M\omega^2}{E_iI_i\beta_i^3}=\frac{1-\cos\beta_i l_i\cosh\beta_i l_i}{\sin\beta_i l_i\cosh\beta_i l_i-\cos\beta_i l_i\sinh\beta_i l_i} \quad . (20)$$

We further assume that the mass of link i is equal to the mass connected, the spatial curve is shown as (c).

(4) Link i is connected with mass m, and connected with mass M at the end.

$$\begin{array}{ll}Y_i''(0)=0 & E_iI_iY_i'''(0)=-\omega_i^2mY(l_i)\\ Y_i''(l_i)=0 & E_iI_iY_i'''(l_i)=-\omega_i^2MY(l_i)\end{array} \quad . . . (21)$$

It can be seen from the modal shape curve that the deformation varies with the position of link. In order to obtain the more sensitive detection data, the vibration sensor should be arranged in a position with large deformation. And the sensor configuration scheme can be determined by using the above method based on the simplification of load and installation fashion. A simpler way is to place vibration sensors at the end of each link, as the end tends to be more deformed under various boundary conditions in a first-order mode shape.

2.3. The collision response of the whole robot

The vibration equation of link i under transverse collision can be described as

$$E_iI_i\frac{\partial^4 y_i(x_i,t)}{\partial x_i^4}+\rho_i\frac{\partial^2 y_i(x_i,t)}{\partial t^2}=q(X_i,t) \quad . . . (22)$$

where $X_i\in(0,l_i)$ is the position collision hit on link i .

The vibration response of the link under collision can be calculated by the following equation

$$y_i(x_i,t)=\begin{array}{l}\sum_{j=1}^{\infty}\frac{1}{\omega_{ij}}\cdot Y_i(x_i)\cdot\int_0^{l_i}Y_i(x_i)\\ \int_0^t q(X_i,\tau)\sin\omega_j(t-\tau)d\tau dx_i\end{array} \quad . . (23)$$

When link 2 is impacted by a force $P\sin\omega t\,\delta(x_2-X_2)$, The response of link 2 can be described as

$$y_2(x_2,t)=\begin{array}{l}PY_2(x_2)Y_2(X_2)\sum_{j=1}^{m_2}\frac{1}{\omega_{2j}^2-\omega^2}\\ (\sin\omega t-\frac{\omega}{\omega_{2j}}\sin\omega_{2j}t)\end{array} \quad . . (24)$$

And the response of links 1 is

$$y_1(x_1,t) = P\cos(\Delta\theta)E_1I_1Y_1(x_1)Y_1(l_1)Y_2'''(0) \\ Y_2(X_2)\sum_{j=1}^{m_2}\frac{1}{\omega_{2j}^2-\omega^2}\sum_{k=1}^{m_1} \\ \frac{1}{\omega_{1k}^2-\omega^2}(\sin\omega t - \frac{\omega}{\omega_{1j}}\sin\omega_{1j}t) \quad (25)$$

where $\Delta\theta$ is the angle between link 1 and link 2. On the other hand, when collision occurred at the point X_1 on link 1, the response of link 1 and 2 can be calculated with

$$y_1(x_1,t) = PY_1(x_1)Y_1(X_1)\sum_{k=1}^{m_1}\frac{1}{\omega_{1k}^2-\omega^2} \\ (\sin\omega t - \frac{\omega}{\omega_{1j}}\sin\omega_{1j}t) \quad . \quad . \quad (26)$$

$$y_2(x_2,t) = P\cos(\theta)E_2I_2Y_2(x_2)Y_2(l_2) \\ Y_1'''(0)Y_1(X_1)\sum_{k=1}^{m_1}\frac{1}{\omega_{1j}^2-\omega^2} \\ \sum_{j=1}^{m_2}\frac{1}{\omega_{2j}^2-\omega^2}(\sin\omega t - \frac{\omega}{\omega_{2j}}\sin\omega_{2j}t) \quad (27)$$

When collision occurred on link 1, its spectrum will resonate at natural frequency ω_{j1}, and link 2 connected to it will resonate at natural frequency ω_{j2}. The amplitude of vibration is related to the magnitude of excitation. The relative magnitude of vibration generated by the collision on link 1 are quite different from those on link 2.

The relative size of the amplitude of the vibration is independent of some experimental conditions, such as the contact position X_1 and the magnitude of the test force P. Therefore, the features selected based on natural frequencies and relative magnitude will effectively guarantee the generalization ability of machine learning algorithms.

Furthermore, the relative amplitude of vibration response in different frequency bands can be used to isolation collision materials, since metal collision has a larger excitation signal bandwidth than human collision.

3. Time-frequency domain feature analysis based on VMD

In this part, the variational mode decomposition (VMD) algorithm is used to analyze the vibration data generated by robot collision, and extract time-domain and frequency-domain features.

The collision experiment is carried out on a platform of a SCARA robot, and as shown in figure 3. Two unidirectional sensors and two-dimensional sensors are mounted on along robot structure. Three collision tests are carried out, the first occurs on link 1 with metal hammer, the second occurs on link 1 with human hand, and the third occurs on link 2 with human hand. The joint, current and vibration data during the experiment are shown in Fig. 4. There is more obvious deviation between collision and non-collision in vibration data than that in current data.

VMD analysis of the three collisions is shown in Fig.6, 7, 8. The data of each sensor is decomposed into 3 IMFs, with the central frequency of around $100Hz$, $800Hz$ and $1300Hz$ respectively, showing good consistency. The time domain signal of each IMF better reflects the relative amplitude among IMFs. So the VMD algorithm can better



Fig. 3. Experiment platform based on SCARA robot

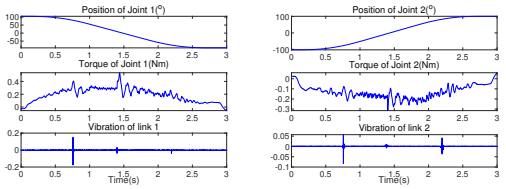


Fig. 4. Current and vibration signals during collision

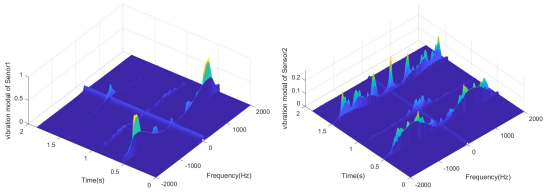


Fig. 5. Frequency diagram of vibration during collision

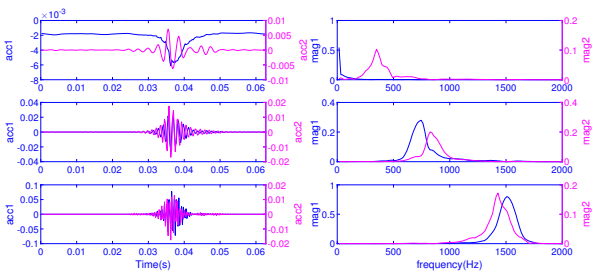


Fig. 6. VMD of vibration signal of collision 1

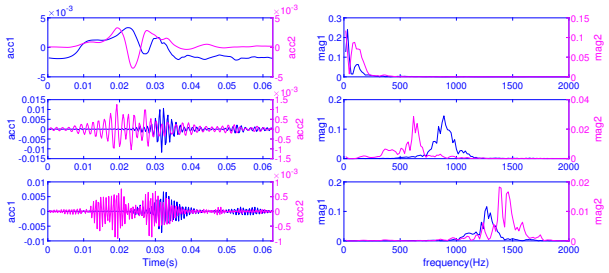


Fig. 7. VMD of vibration signal of collision 2

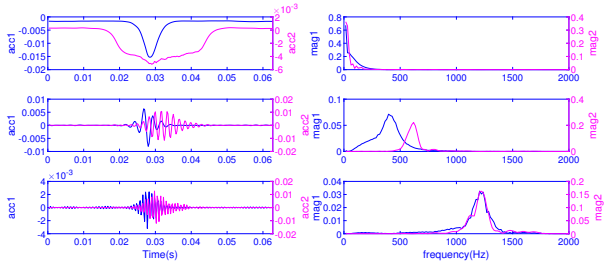


Fig. 8. VMD of vibration signal of collision 3

extract the modal features compared with FFT method.

4. Experiment and Result

Based on the vibration features discussed above, we proposed a neural network algorithm for monitoring of collisions. A sliding time window of 0.1 second is set to sample vibration data of each sensor, and the collision related symptoms are extracted from VMD analysis, and then used for collision detection and isolation neural network algorithm. The collision detection network together with the VMD algorithm should be executed within each sliding window. Once a collision event was detected, the collision location and isolation network is launched with the current vibration modal data. The procedure of the algorithm is shown in Fig. 10.

For the collision link isolation NN, the samples are labeled as [1,0,0], [0, 1,0] and [0,0,1] for collision occurred on base, link 1 and link 2, respectively. The structure of the neural network is 25-10-3. For the isolation of collision material, we collected the vibration data of sensor nearby the link where collision occurred. The samples are labeled as [1, 0] and [0, 1] for the collision excited by steel hammer and human hand, respectively. The structure of the neural network is 25-10-2, and Levenberg-marquardt training algorithm is used to train the like isolation and material isolation network.

As shown in figure 10, there are 4 collisions in this process, collision 1 and 3 occurs on link 2, and collision 2 and 4 occurs on link 1. The first two are human hand collisions, and the last two are metal tool collisions.

It can be seen that the collision modes significantly

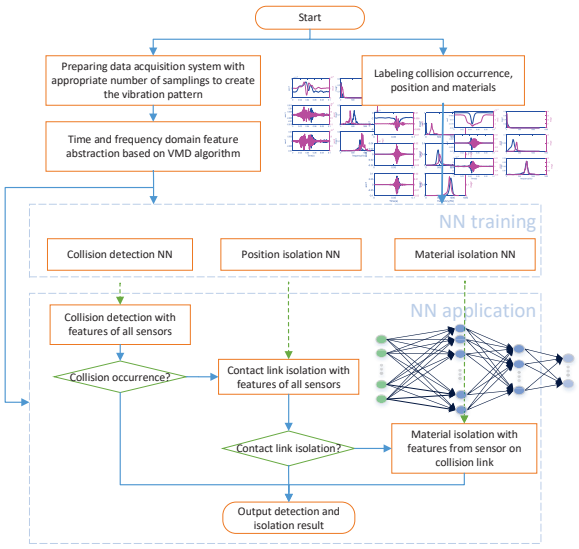


Fig. 9. Operation procedure of collision detection and isolation

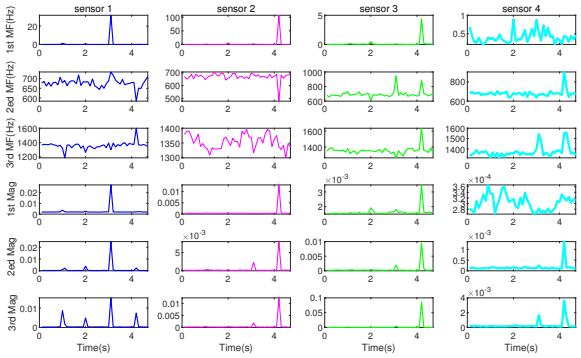


Fig. 10. Features abstraction based on VMD algorithm

change when a collision occurs, and the mode shape characteristic of the relative size of different sensors is consistent with the collision characteristics discussed above. Fig.11 shows the outputs of the networks.

The performance of the proposed algorithm is further analyzed in this part. For the first experiment, the proposed method is compared with the direct current estimation method[2]. As it shows in Fig.12, there are four collisions in the experiment, and it can be seen that the calculation of the dynamic model is in good agreement with the current signal. However, when the joint velocity is close to 0, the error of estimation become nonnegligible. This is due to the uncertainty of the friction model, which is common in traditional industrial robots.

The central frequency and modal characteristics of the vibration signals do not change significantly. As it shows in Fig. 13, the central frequencies of the second and third IMF in the vertical experiment are 800 and 1500Hz, respectively, which is consistent with horizontal experiment. The central frequence of first IMF is low, reflecting the spectrum of the robot's active motion, and has little to

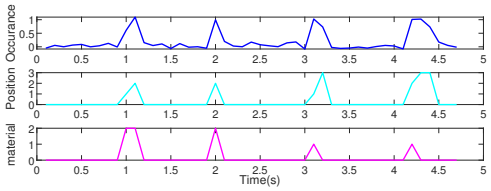


Fig. 11. Outputs of neural networks

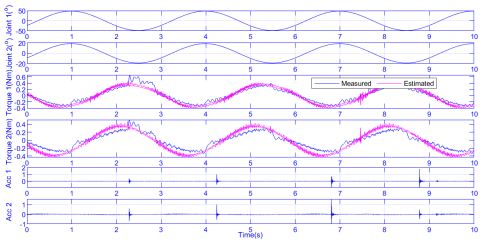


Fig. 12. Current and vibration in vertical placement test

do with the collision vibration. On the other hand, the relative size of maximum amplitude among the second and the third IMF also reflects the characteristics of robot collision vibration discussed in section II. It can be predicted that the proposed method has better robustness in the situation of load variation or inclination of base.

5. Conclusion

This paper presents a robot collision monitoring method based on vibration signal. Firstly, the key features of collision detection are analyzed based on the robot dynamics model. Secondly, VMD algorithm is used to extract the time-frequency characteristics of the collisions. At last, SCARA robot and six joints robot is used to verify the method. The contribution of this paper is as follows, firstly, this method does not depend on the accurate dynamic model, and has good sensitivity, especially short time collision. Secondly, the proposed method has

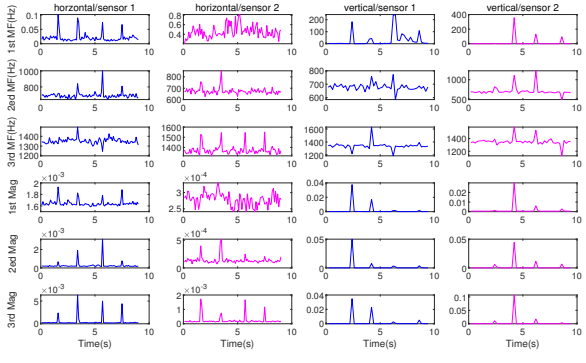


Fig. 13. Features in horizontal VS vertical placement test

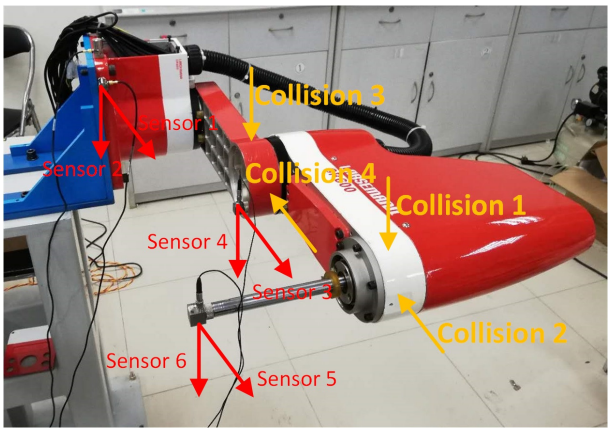


Fig. 14. The vertical placement test

good robustness, and still has good detection effect when the load changes and friction changes. In addition, this method can provide information of collision in many aspects, including collision location, collision material.

References:

[1] J. Vorndamme, M. Schappler, S. Haddadin, Collision detection, isolation and identification for humanoids, 2017.

[2] S. Haddadin, A. D. Luca, A. Albu-Schaffer, Robot collisions: A survey on detection, isolation, and identification, IEEE Transactions on Robotics PP (99) (2017) 1–21.

[3] Luca A D , Albu-Schaffer A , Haddadin S , et al. Collision Detection and Safe Reaction with the DLR[C]. Intelligent Robots and Systems, 2006 IEEE/RSJ International Conference on. IEEE, 2006.

[4] S. Lu, J. H. Chung, S. A. Velinsky, Human-robot collision detection and identification based on wrist and base force torque sensors, in: IEEE International Conference on Robotics & Automation, 2006.

[5] F. Caccavale, A. Marino, G. Muscio, F. Pierri, Discrete-time framework for fault diagnosis in robotic manipulators, IEEE Transactions on Control Systems Technology 21 (5) (2013) 1858–1873.

[6] Y.Yamada, Y. Hirasawa, S. Huang, Y. Umetani, K. Suita, Human-robot contact in the safeguarding space, IEEE/ASME Transactions on Mechatronics 2 (4) (2002) 230–236.

[7] Wagner M , Liu S , Giusti A , et al. Interval-Arithmetic-Based Trajectory Scaling and Collision Detection for Robots with Uncertain Dynamics[C]. IEEE International Conference on Robotic Computing. IEEE, 2018.

[8] Sharkawy A N , Koustoumpardis P , Aspragathos N A . Human-Robot Collisions Detection for Safe Human-Robot Interaction Using One Multi-Input-Output Neural Network[J]. Soft Computing, 2019, 24(9),6687–6719.

[9] M.Feiyan. W.Gao, L Ning. Collision detection and identification on robot manipulators based on vibration analysis, Sensors 19 (2019) 1080.

[10] A. Caldas, M. Makarov, M. Grossard, P. Rodriguez-Ayerbe, D. Dumur, Adaptive residual filtering for safe human-robot collision detection under modeling uncertainties, in: IEEE/ASME International Conference on Advanced Intelligent Mechatronics, 2013.

[11] M. Makarov, A. Caldas, M. Grossard, P. Rodriguez-Ayerbe, D. Dumur, Adaptive filtering for robust proprioceptive robot impact detection under model uncertainties, IEEE/ASME Transactions on Mechatronics 19 (6) (2014) 1917–1928.

[12] A. Baradaran, J. Kuehn,S. Haddadin, Observer-Extended Direct Method for Collision Monitoring in Robot Manipulators Using Proprioception and IMU Sensing, IEEE Robotics and Automation Letters 5 (2) (2020) 954–961.

[13] Chan L , Naghdy F , Stirling D. Extended active observer for force estimation and disturbance rejection of robotic manipulators[J]. Robotics & Autonomous Systems, 2013, 61(12):1277-1287.

[14] Rafezy B , Howson W P. Exact dynamic stiffness matrix for a thin-walled beam of doubly asymmetric cross-section filled with shear sensitive material[J]. International Journal for Numerical Methods in Engineering, 2010, 69(13):2758-2779.